LA-UR-18-28942
Approved for public release; distribution is unlimited.

Title: Nanoindentation Characterization of FeCrAl C26M Welds

Author(s): Gigax, Jonathan Gregory
Li, Nan

Intended for: Report

Issued: 2018-09-20

Nanoindentation Characterization of FeCrAl C26M Welds

Fuel Cycle Research & Development

Prepared for
U.S. Department of Energy
Advanced Fuels Campaign

Jonathan G. Gigax
Nan Li

8/24/18

SUMMARY

The present report summarizes the initial mechanical characterization of a welded FeCrAl alloy, C26M, with comparison to two other welded specimens, C35M and C37M. The welded C26M showed a larger fusion and heat-affected zone than either the C35M or C37M welds. Nanoindentation hardness measurements using a Berkovich tip showed no major changes in the hardness and modulus between the fusion zone, heat-affected zone, and unaffected C26M tube. Nanoindentation strain-rate sensitivity tests were also performed and showed no changes between each of the regions in the C26M weld. Spherical nanoindentation tests were carried out to evaluate the nanoindentation modulus and nanoindentation yield strength in each of the regions of the C26M weld sample. No significant changes in strength from welding were observed with an average nanoindentation yield strength of ~1 GPa and nanoindentation modulus of ~220 GPa. Nanoindentation tests all show that the C26M does not change significantly after welding and that further characterization with some form of tensile loading is necessary to determine if any significant change has occurred.

TABLE OF CONTENTS

FIGURES

TABLES

Intentionally Blank

1. Introduction

Among several candidates for "accident tolerant" fuel cladding, FeCrAl alloys are among the top choices due to their superior high temperature oxidation resistance, aqueous corrosion resistance, low radiation-induced swelling, and tolerance to loss-of-coolant accident conditions [1-4]. Despite their higher neutron absorption cross-section compared to zirconium-based alloys, their mechanical and chemical stability over a range of environment make this alloy and attractive candidate to others (i.e. SiC-based cladding). The ongoing work led by Oak Ridge National Lab has targeted an optimized FeCrAl alloy for tube processing and implementation in light water reactors [5]. Since both tubing and connectors cannot be made (reasonably) from a single monolithic structure, separate components must be joined together. Welding is a common technique that ensures good high temperature performance but causes microstructural changes to the welded components with two new unique regions forming after processing: a fusion zone (FZ) and heat-affected zone (HAZ). Previous examination of welded FeCrAl alloys, C35M and C37M, showed some degradation in the strength of the material and a dramatic decrease in the ductility [6]. Nanoindentation analysis was used to probe local property changes on the microscale and was able to produce similar trends to the larger scale tensile tests [7]. In this report, we utilize nanoindentation to perform initial characterization of a welded FeCrAl C26M tube.

2. Materials and Methods

A FeCrAl C26M tube was welded using conventional tungsten inert gas (TIG) processing with argon as the cover gas. Tubing was sectioned from the weld and specimens polished on the longitudinal surface of the tube. To ensure that regions outside of the heat-affected zone were included in the sample, at least 3 mm of tubing was included in each sample. All specimens were ground using successive SiC grit papers down to a grit of 1200. Samples were then polished first using a 0.25 μm diamond solution and finished with a 0.04 μm silica solution. Table 1 provides the composition of the C26M tubing examined in this report.

Table 1. Chemical composition of FeCrAl C26M alloy.

Alloy ID	Fe	Cr	Al	Y	Mo	Si	Nb	C	S	O	N
C26M	80.72	13.01	6.24	0.030	-	-	-	<0.01	0.001	-	-

Scanning electron microscopy of the polished tubes was performed in a FEI Inspect equipped with an EDAX system for acquiring electron backscatter diffraction patterns (EBSD), and obtained with an electron energy of 20 keV. Nanoindentation tests were performed on a Keysight G200 Nanoindenter with a diamond, pyramidal (Berkovich) tip to a final displacement of 1,000 nm, a constant strain rate (loading rate divided by the load) of 0.05 s^{-1}. Continuous stiffness measurements (CSM) were performed at a frequency of 45 Hz and 2 nm displacement amplitude. Hardness and modulus measurements were determined using the Oliver-Pharr method [8]. The tip area function was calibrated by indenting fused silica and using tip properties with a Young's modulus and Poisson's ratio of 1130 GPa and 0.07 (diamond). Strain-rate sensitivity measurements were made using a Berkovich tip with a base strain rate of 0.1 s^{-1}. The indenter tip was displaced up to 1000 nm into the surface before performing the first strain rate change to 0.001 s^{-1} over a depth of 150 nm, followed by a second strain rate change to 0.01 s^{-1}. Between each strain-rate jump, indentation at the base strain rate occurred over a depth of 150 nm. Spherical nananoindentation tests were performed using a 100 μm radius tip. Nanoindentation was performed to a depth of 500 nm using similar system parameters to the nanoindentation with a Berkovich tip.

3. Results and Discussion

3.1 Nanoindentation

Figure 1 provides an inverse pole figure (IPF) map of the welded C26M tube and C37M samples for comparison. It is worth noting that the C26M weld joins two FeCrAl materials in two different forms: bar and tube. The more random oriented region on the left-side of the weld is associated with the bar stock. Compared to the C37M and C35M welds, the fusion and heat-affected zones are wider in the C26M weld. For the purpose of this initial characterization, only the tube side of the C26M weld was performed.

Fig. 2 provides a comparison of representative nanoindentation hardness and modulus curves of the C26M weld in each of the three regions as a function of depth. Nanoindentation was performed with an array of 42 x 2 indents starting in the fusion zone and ending in the bulk material (BM) with a spacing of 50 μm in the x-direction and 75 μm in the y-direction. Two sets of these indents were performed in the C26M tube to achieve good sampling across the material. For the purpose of comparison, only one set of indents were conducted in the C35M and C37M specimens. Nanoindentation hardness and modulus values presented in Fig. 3 are averaged between a depth range of 400-500 nm.

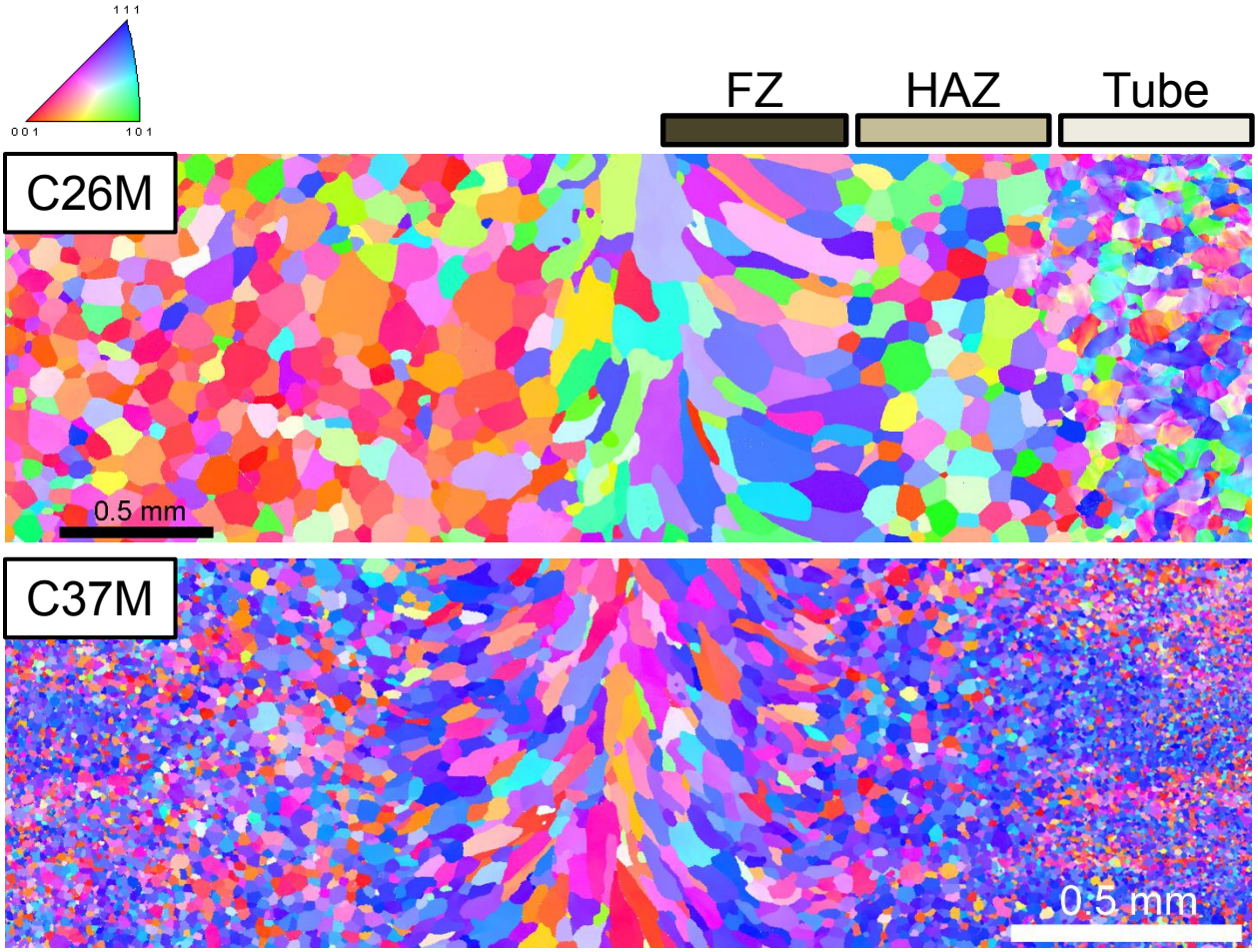

Figure 1 - Inverse pole figure map of the FeCrAl C26M and C37M weld. Labels for the fusion zone (FZ), heat-affected zone (HAZ) and C26 tube region provided.

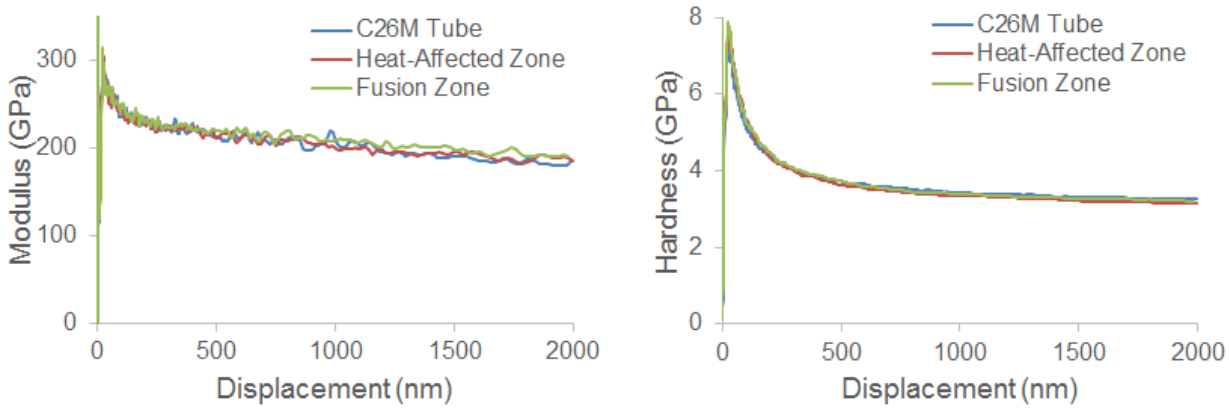

Figure 2 – Representative nanoindentation (a) modulus and (b) hardness data for the welded C26M tube in the fusion zone, heat-affected zone, and tube, respectively.

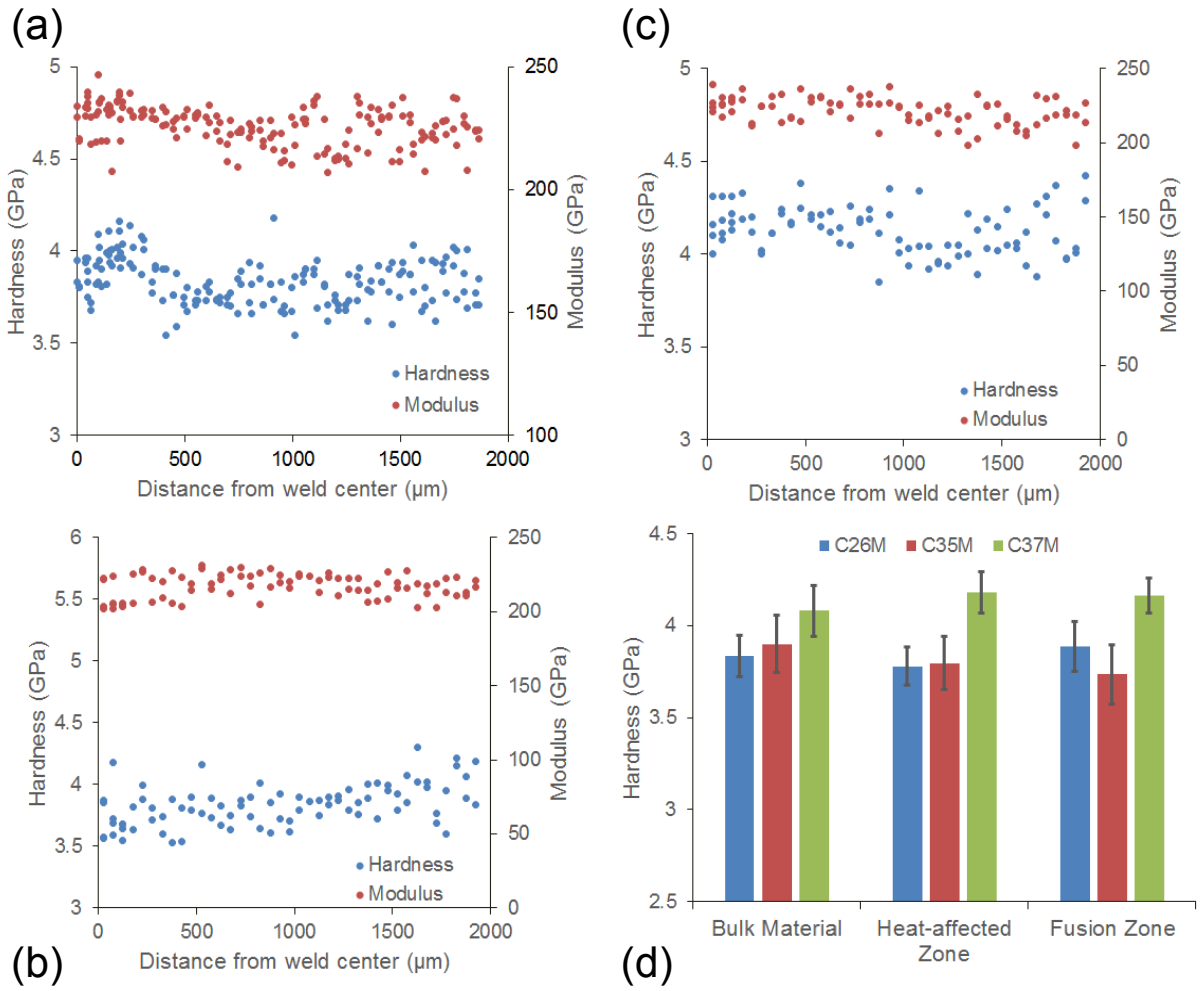

Figure 3 - Nanoindentation hardness and modulus profile in the welded (a) C26M tube, (b) C35M3, and (c) C37M. (d) Comparison of the hardness in each of the regions for each of the three weld specimens. The weld center for the C26M tube is defined in Fig. 1 as the features corresponding to the left edge of the FZ marker.

Figure 3a shows the hardness and modulus profile, as a function of distance from the weld center, in the C26M sample. A slight increase in the hardness ~100-200 μm from the weld center is present and consistent across the two indentation sets. Beyond this small peak, the hardness and modulus both appear flat across the sample. No significant changes in the modulus were observed. The C35M specimen (Fig. 3b) exhibited a ~10% lower hardness in the weld region than in the bulk material, indicative of weld softening and similar to previously measured values [6,7]. Fig. 3c shows that the C37M specimen possesses no significant changes in hardness or modulus across the specimen, in good agreement with previous results. Fig. 2d compares the differences in hardness between the C26M, C35M, and C37M in each of the regions. Table 2 summarizes the Berkovich nanoindentation results.

Table 2. Summary of nanoindentation data obtained using a Berkovich tip. Hardness and modulus values averaged over a displacement range of 400-500 nm. Error bars denote one standard deviation.

	Modulus (GPa)			Hardness (GPa)		
	Bulk Material	**Heat-affected Zone**	**Fusion Zone**	**Bulk Material**	**Heat-affected Zone**	**Fusion Zone**
C26M	225.01 ± 7.59	221.78 ± 7.66	230.35 ± 6.3	3.83 ± 0.11	3.78 ± 0.1	3.89 ± 0.13
C35M	217.32 ± 6.43	220.6 ± 7.9	212.85 ± 10.15	3.90 ± 0.15	3.80 ± 0.14	3.74 ± 0.16
C37M	217.38 ± 8.74	226.74 ± 7.68	224.66 ± 7.24	4.08 ± 0.14	4.18 ± 0.11	4.16 ± 0.09

Since the C26M weld specimen showed no significant differences across each region, one additional test was performed to determine if any other significant changes had occurred in the microstructure. The nanoindentation strain-rate jump test was recently developed by Meyer et al. and shown to obtain strain-rate sensitivity (m) values close to that from uniaxial tests [10]. Although the strain rate sensitivity can be used to determine the type of creep in a system, this information is of limited value for FeCrAl materials at room temperature. More relevant to the analysis, the value is inversely proportionate to the activation volume which is influenced by the presence of defects in the system [11]. For the weld specimen, changes in the strain rate sensitivity can be inferred to be changes in the microstructure or defect density that influence the stress activation volume.

Fig. 4a shows representative nanoindentation strain rate jump tests in each of the regions in the C26M weld specimen. Nanoindentation strain rate jump tests were conducted at a depth where hardness values are nearly constant, or at ~1000 nm. Fig. 4b shows the strain rate sensitivity (SRS) values as a function of distance from the center of the weld and Table 3 summarizes the SRS values. From the data, there are no significant changes in the SRS values in each of the regions.

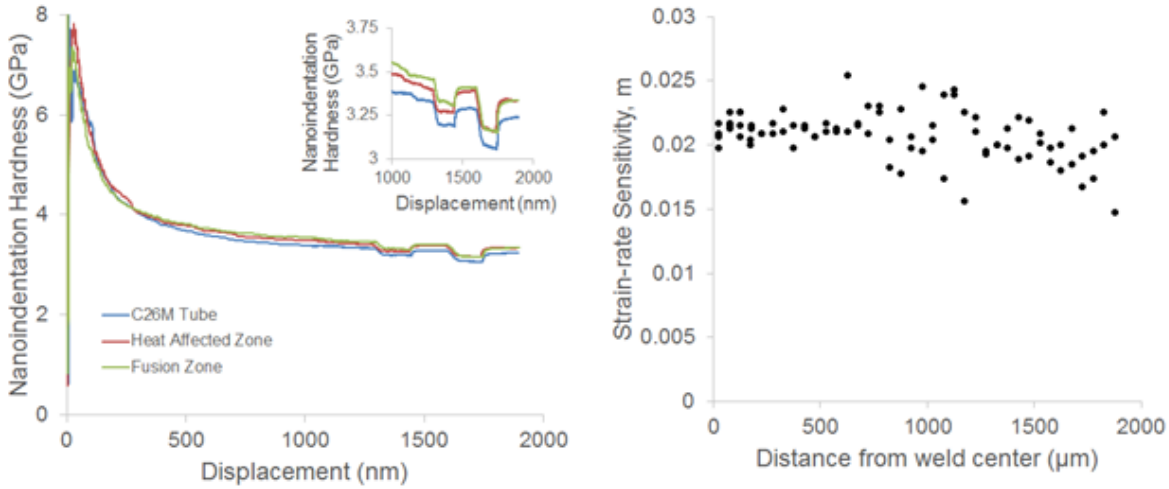

Figure 4 - Plots of the (a) nanoindentation hardness with strain rate jump tests and (b) strain-rate sensitivity profile as a function of the distance from the weld center.

Table 3 – Summary of nanoindentation data obtained using a Berkovich tip. Hardness and modulus values averaged over a displacement range of 400-500 nm. Error bars denote one standard deviation.

	C26M Tube	Heat-affected Zone	Fusion Zone
Strain Rate Sensitivity, m	0.0196 ± 0.0018	0.0212 ± 0.0023	0.0212 ± 0.0008

3.2 Spherical Nanoindentation

For spherical nanoindentation characterization, our principle interest is to determine if any significant changes between each region in the weld specimen exists during elastic loading. Since the grain sizes of the tube and weld regions are quite large (>50 μm), indentation using a large tip radii will only probe a volume containing only one or two grains.

Fig. 5a provides typical nanoindentation stress-strain curves for the C26M weld specimen, calculated using a process outlined elsewhere [9]. The differences between the curves, especially at low strain values, is not significant. Based on the results from the Berkovich nanoindentation, the trend in Fig. 4a is not surprising. However, to ensure that this result is representative of the whole weld, 84 indents were placed with at least 20 indents per region. Fig. 5b shows a comparison of the nanoindentation yield strength between each region in the C26M, C35M, and C37M, respectively. Table 4 summarizes the spherical nanoindentation results.

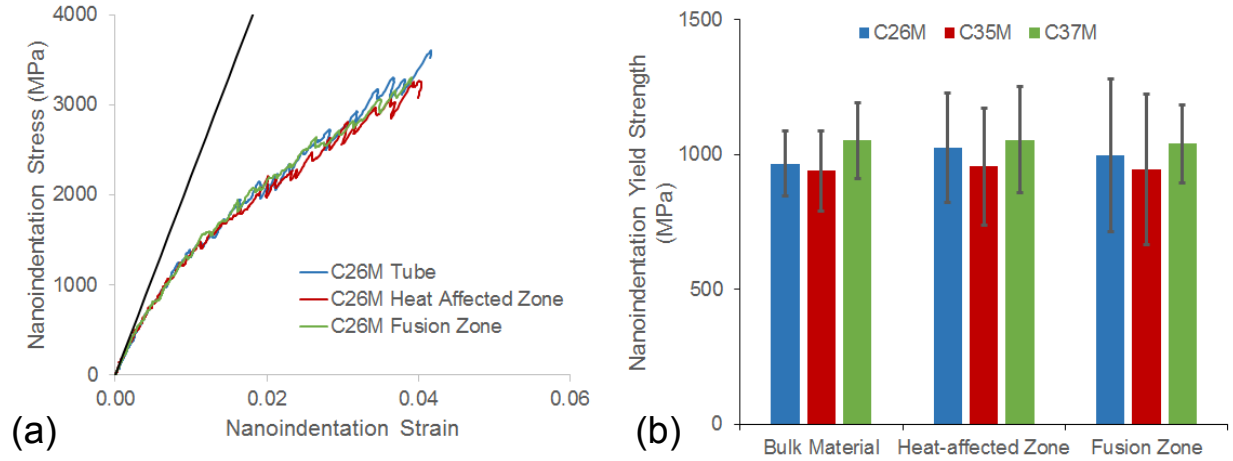

Figure 5 – (a) Representative 100 μm spherical nanoindentation stress-strain curves for the fusion zone, heat-affected zone, and tube region of the C26M welded tube. (b) Comparison of the nanoindentation yield strength for the C26M, C35M, and C37M weld samples.

Table 4 – Summary of spherical nanoindentation modulus and nanoindentation yield strength obtained from a 100 μm tip for the C26M, C35M, and C37M welds. Error bars denote one standard deviation.

	Nanoindentation Modulus (GPa)			Nanoindentation Yield Strength (MPa)		
	Bulk Material	**Heat-affected Zone**	**Fusion Zone**	**Bulk Material**	**Heat-affected Zone**	**Fusion Zone**
C26M	220.4 ± 3.79	218.31 ± 6.13	220.02 ± 3.54	965.39 ± 119.28	1024.76 ± 204.02	996.36 ± 284.75
C35M	218.65 ± 2.64	218.44 ± 2.45	215.08 ± 5.22	939.35 ± 148.12	954.0 ± 216.43	944.05 ± 279.15
C37M	217.86 ± 2.49	215.81 ± 3.86	216.46 ± 4.73	1051.2 ± 141.2	1052.9 ± 196.93	1038.6 ± 145.48

From the spherical nanoindentation results, no significant differences are observed in the C26M weld between each region. The nanoindentation yield strength and nanoindentation modulus were calculated to be ~1 GPa and ~220 GPa, respectively. Both the C35M and C37M also possess similar trends with the C26M. Although the average nanoindentation yield strength for the C37M is slightly higher than that of the C26M and C35M and in agreement with the nanoindentation hardness results, the difference is not significant. There is a slight disagreement with the nanoindentation hardness measurements which showed a very small change (10%) in the hardness from the FZ to the BM in the C35M weld. We note that the process of calculating spherical indentation stress-strain curves can result in large variations in the nanoindentation yield strength within a single indent. Further coupled with differences in orientation can give rise to this apparent discrepancy.

Conversion to a uniaxial yield strength can be calculated by [12],

$$\sigma = \frac{\sigma_{ind}}{2.2}$$

Where σ_{ind} is the nanoindentation stress state and σ is the uniaxial stress state. By applying this conversion factor, the nanoindentation yield strengths calculated here closely match the expected yield strength in uniaxial tests.

4. Conclusions and Future Work

In this study, we have performed an initial characterization of the microstructure of a C26M weld performed by a conventional TIG welding process. The nanoindentation hardness and modulus measured by a Berkovich tip was ~3.8 GPa and ~225 GPa, respectively. No significant differences in hardness and modulus were observed between the fusion zone, heat-affected zone, and bulk material. Comparison with previously characterized C35M and C37M welds show similar trends, with the only difference observed in the C35M weld hardness. Strain-rate jump tests were performed on the C26M weld to characterize changes in the strain rate sensitivity. Across the specimen, no significant changes in the SRS value were measured. Spherical nanoindentation was also performed to evaluate the nanoindentation modulus and yield strength. The C26M was found to have a nanoindentation modulus and yield strength of ~220 GPa and ~1 GPa, respectively. Both the C35M and C37M welds had similar values.

One of the major drawbacks to the nanoindentation is the limited information obtained on the relevant properties that change after welding. While some adjustments to the hardness and nanoindentation yield strength can be made to obtain a yield strength closer to uniaxial values, information on properties such as ductility or fracture toughness are not provided by the test for otherwise ductile materials. As the focus for our future work, we have utilized laser machining for rapid fabrication of cantilever specimens. Fig. 6 shows an SEM overview of the cantilevers. Although some focused ion beam cleanup is required to achieve specified cantilever dimensions, performing micro-cantilever testing in each of the regions enables the extraction of fracture toughness and gaining additional insight into material property change across the weld regions.

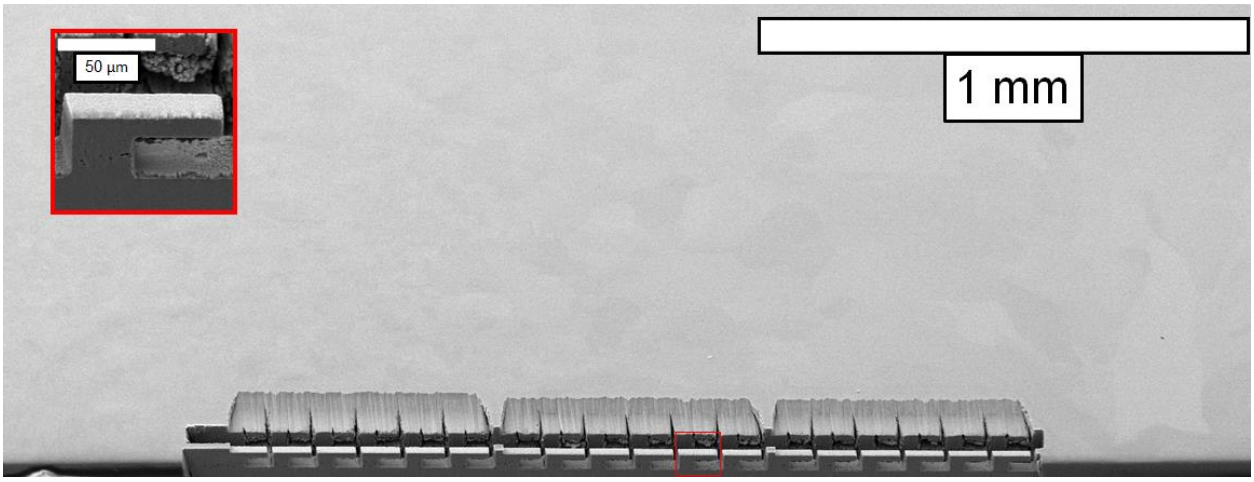

Figure 6 - SEM overview of micro-cantilevers fabricated in the C26M weld specimen.

5. References

[1] R.B. Rebak, K.A. Terrani, W.P. Gassmann, J.B. Williams, K.L. Ledford. Improving Nuclear Power Plant Safety with FeCrAl Alloy Fuel Cladding, MRS Advances (2017) 1-8.
[2] Y. Yamamoto, B.A. Pint, K.A. Terrani, K.G. Field, Y. Yang, L.L. Snead. Development and property evaluation of nuclear grade wrought FeCrAl fuel cladding for light water reactors, J Nucl Mater 467, Part 2 (2015) 703-716.
[3] K.G. Field, M.N. Gussev, Y. Yamamoto, L.L. Snead. Deformation behavior of laser welds in high temperature oxidation resistant Fe–Cr–Al alloys for fuel cladding applications, J Nucl Mater 454 (2014) 352-358.
[4] S.J. Zinkle, K.A. Terrani, L.L. Snead. Motivation for utilizing new high-performance advanced materials in nuclear energy systems, Current Opinion in Solid State and Materials Science 20 (2016) 401-410.
[5] Y. Yamamoto, Z. Sun, B.A. Pint, K.A. Terrani. Optimized Gen-II FeCrAl cladding production in large quantity for campaign testing. Oak Ridge: Oak Ridge National Laboratory, 2016.
[6] M.N. Gussev, K.G. Field, Y. Yamamoto. The analysis of the general performance and mechanical behavior of unirradiated FeCrAl alloys before and after welding. Oak Ridge, TN: Oakridge National Laboratory, 2016.
[7] J. Weaver, E. Aydogan, N. A. Mara, S. A. Maloy, Nanoindentation of electropolished FeCrAl alloy welds, Los Alamos, NM: Los Alamos National Lab, 2017.
[8] W.C. Oliver, G.M. Pharr. Measurement of hardness and elastic modulus by instrumented indentation: Advances in understanding and refinements to methodology, J Mater Res 19 (2004) 3-20.
[9] S. Pathak, S. R. Kalidindi. Spherical nanoindentation stress-strain curves. Mater. Sci. Eng. R 91 (2015) 1-36.
[10] V. Maier, K. Durst, J. Mueller, B. Backes, H. W. Hoppel, M. Goken, Nanoindentation strain-rate jump tests for determining the local strain-rate sensitivity in nanocrystalline Ni and ultrafine-grained Al, J. Mater. Res. 26 (2011) 1421-1430.
[11] Y. M. Wang, A. V. Hamza, E. Ma, Temperature-dependent strain rate sensitivity and activation volume of nanocrystalline Ni. Acta Mater. 54 (2006) 2715-2726.
[12] D.K. Patel, S.R. Kalidindi. Correlation of spherical nanoindentation stress-strain curves to simple compression stress-strain curves for elastic-plastic isotropic materials using finite element models. Acta Mater. 112 (2016) 295-302.